Cell Reports

Article

# *Arabidopsis* phospholipase Dζ2 facilitates vacuolar acidification and autophagy under phosphorus starvation by interacting with VATD

## Graphical abstract

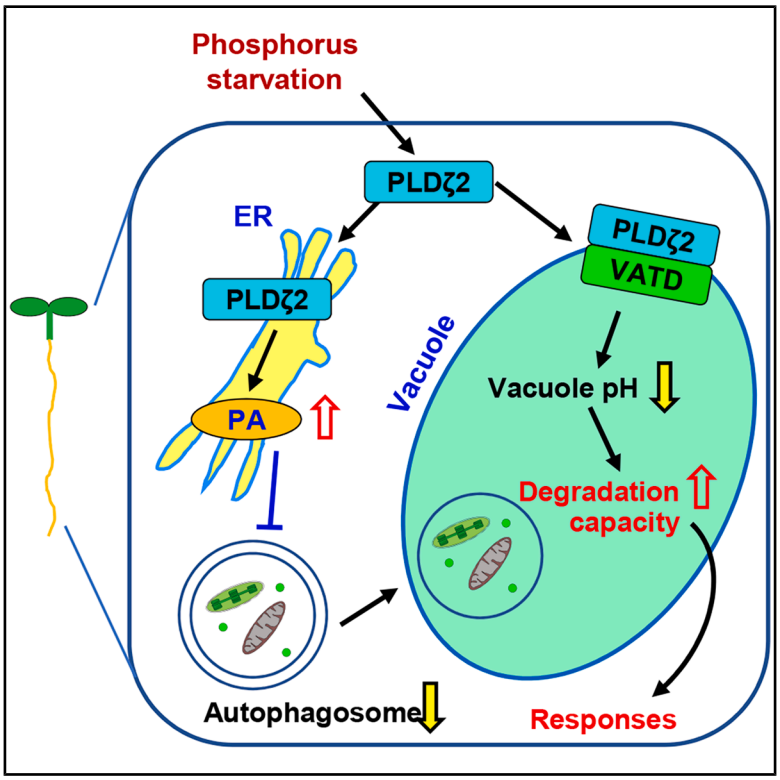


## Highlights

- PLDζ2 deficiency leads to impaired autophagic flux and vacuolar defects
- PLDζ2 promotes vacuolar acidification and autophagy under phosphorus deficiency
- PLDζ2 interacts directly with V-ATPase subunit D to enhance vacuolar acidification
- Vacuolar pH is crucial for autophagic activity

## Authors

Bin Guan, Ke-Xuan Xie, Xin-Qiao Du, ..., Wen-Hui Lin, Jiří Friml, Hong-Wei Xue

## Correspondence

hwxue@sjtu.edu.cn

## In brief

Guan et al. show that *Arabidopsis* phospholipase Dζ2 (PLDζ2) facilitates vacuolar acidification by interacting with V-ATPase subunit D (VATD) to promote autophagy under phosphorus starvation. PLDζ2 deficiency disrupts vacuolar function and impairs autophagic flux, highlighting the critical role of vacuolar pH in autophagy regulation.

Guan et al., 2025, Cell Reports *44*, 116024
July 22, 2025 
https://doi.org/10.1016/j.celrep.2025.116024

CellPress

Cell Reports

CellPress
OPEN ACCESS

Article

# *Arabidopsis* phospholipase Dζ2 facilitates vacuolar acidification and autophagy under phosphorus starvation by interacting with VATD

Bin Guan,[1,2] Ke-Xuan Xie,[1] Xin-Qiao Du,[1] Yu-Xuan Bai,[3] Peng-Chao Hao,[1] Wen-Hui Lin,[3] Jiří Friml,[2] and Hong-Wei Xue[1,4,5,*]

[1]Shanghai Collaborative Innovation Center of Agri-Seeds, School of Agriculture and Biology, Shanghai Jiao Tong University, Shanghai 200240, China

[2]Institute of Science and Technology Austria (ISTA), Klosterneuburg, Austria

[3]The Joint International Research Laboratory of Metabolic and Developmental Sciences, Joint Center for Single Cell Biology, School of Life Sciences and Biotechnology, Shanghai Jiao Tong University, Shanghai 200240, China

[4]Guangdong Laboratory for Lingnan Modern Agriculture, Guangdong Basic Research Center of Excellence for Precise Breeding of Future Crops, College of Agriculture, South China Agricultural University, Guangzhou 510642, China

[5]Lead contact

*Correspondence: hwxue@sjtu.edu.cn

https://doi.org/10.1016/j.celrep.2025.116024

## SUMMARY

Vacuolar acidification is crucial for the homeostasis of intracellular pH and the recycling of proteins and nutrients in cells, thereby playing important roles in various physiological processes related to vacuolar function. The key factors regulating vacuolar acidification and underlying mechanisms remain unclear. Here, we report that *Arabidopsis* phospholipase Dζ2 (PLDζ2) promotes the acidification of the vacuolar lumen to stimulate autophagic degradation under phosphorus deficiency. The *pldζ2* mutant massively accumulates autophagic structures while exhibiting premature leaf senescence under nutrient starvation. Impaired autophagic flux, lytic vacuole morphology, and lytic degradation in *pldζ2* indicate that PLDζ2 regulates autophagy by affecting the vacuolar function. PLDζ2 locates in both tonoplast and cytoplasm. Genetic, structural, and biochemical studies demonstrate that PLDζ2 directly interacts with vacuolar-type ATPase (V-ATPase) subunit D (VATD) to promote vacuolar acidification and autophagy under phosphorus starvation. These findings reveal the importance of V-ATPase and vacuolar pH in autophagic activity and provide clues in elucidating the regulatory mechanism of vacuolar acidification.

## INTRODUCTION

Vacuoles are the most prominent membrane-bound organelles in plant cells and are crucial for growth and development, as well as the response to environmental stimuli.[1–4] Vacuolar-type ATPases (V-ATPases), initially identified in yeast and plant tonoplasts, are membrane-embedded protein complexes that function as ATP-driven proton pumps and contribute to the acidification and maintenance of the pH of intracellular compartments, thus playing important roles in various cellular processes, including protein processing and degradation through endocytosis or autophagy pathways.[5–9] The V-ATPases complexes are composed of the peripheral V1 domain (responsible for ATP hydrolysis) and the membrane-embedded V0 domain (responsible for proton translocation).[6] The V1 domain consists of 8 subunits (VHA-A to -H), and the V0 domain consists of 5 subunits (VHA-a, -c, -c″, -d, and e).[10] In yeast cells, phosphatidylinositol phosphate (PIP) lipids interact with V-ATPase subunit isoforms to affect the organelle pH.[11–14] However, it is still unknown whether and how phospholipase or structural phospholipids are involved in the regulation of vacuolar acidification.

Phospholipase D (PLD) is a type of phosphate ester hydrolase that acts on various ester bonds of phospholipid molecules. PLD is highly conserved in plants and animals and hydrolyzes the structural phospholipids phosphatidylcholine (PC), phosphatidylethanolamine (PE), and phosphatidylglycerol (PG) to generate phosphatidic acid (PA), an important signaling molecule regulating various physiological processes.[15,16] The *Arabidopsis* genome encodes 12 *PLD* genes, which are classified into six subtypes based on sequence similarity and biochemical characteristics. *PLDζ1* and *PLDζ2* are highly expressed in the root, and transcription of *PLDζ2* is significantly increased upon nitrogen and phosphorus starvation.[17,18]

Autophagy refers to the highly conserved process in eukaryotes, which involves the transporting of dysfunctional organelles or biological macromolecules (lipids, proteins, etc.) to vacuoles via membrane-bilayer-encapsulated autophagosomes.[19,20] In *Arabidopsis*, autophagy-deficient mutants exhibit hypersensitivity to nutrient deprivation, premature leaf senescence, and a shortened life span.[21–23] The autophagic flux involves autophagosome formation, maturation, fusion with vacuoles, subsequent degradation, and release of macromolecules back into

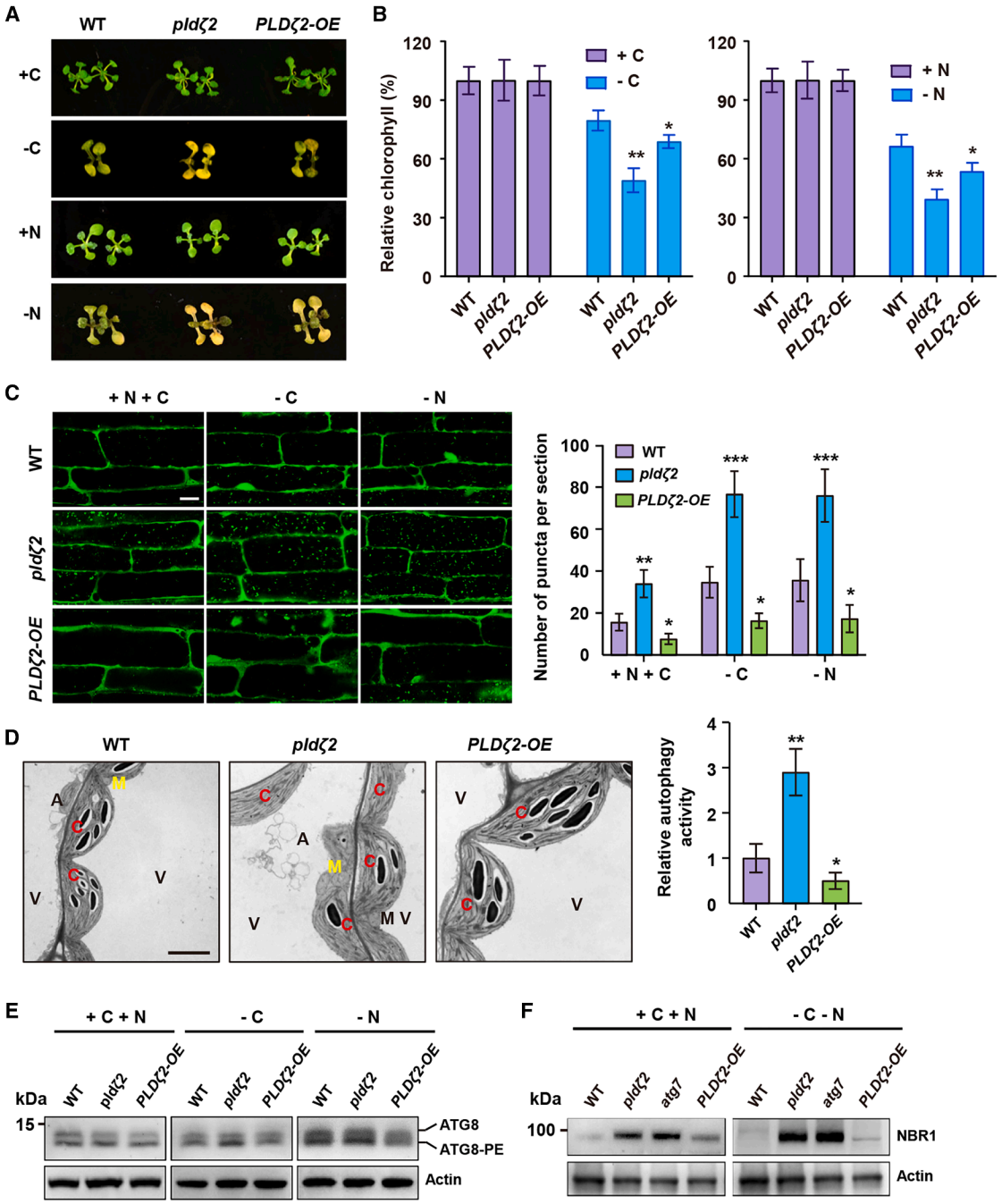


**Figure 1. Autophagic flux was blocked in *pldζ2* mutant**

(A and B) Phenotypic observation (A) and measurement of chlorophyll contents (B) of WT, *pldζ2* mutant, and *Arabidopsis* seedlings overexpressing PLDζ2 (*PLDζ2-OE*) upon carbon or nitrogen starvation. Seedlings were grown on Murashige and Skoog (MS) medium for 1 week and then transferred to MS medium with (+C) or without (–C) sucrose, followed by constant dark treatment, or MS medium with (+N) or without nitrogen (–N) under normal growth conditions. Relative chlorophyll contents were calculated by comparing the values of –C or –N seedlings to those of +C or +N conditions. Experiments were biologically repeated three times, and data are mean ± SD ($n = 15$). Statistical significance was determined by Student's t test (*$p < 0.05$ and **$p < 0.01$; compared to WT at same condition). (C) Observation of GFP-ATG8e-labeled dots and ring-like structures (left, bars: 50 μm) and calculation of puncta numbers per root section (right) in WT, *pldζ2*, and *PLDζ2-OE* seedlings upon carbon or nitrogen starvation. *Arabidopsis* seedlings expressing GFP-ATG8e fusion protein were grown on 1/2 MS medium for 5 days and then transferred to 1/2 MS medium with or without carbon or nitrogen and visualized by confocal microscopy. Experiments were biologically repeated three times, and data are mean ± SD ($n = 15$). Statistical significance was determined by Student's t test (*$p < 0.05$, **$p < 0.01$, and ***$p < 0.001$; compared to WT at same condition).

*(legend continued on next page)*

cytosol, and defects in autophagic flux contribute to neurodegeneration, cancer, myopathy, cardiovascular diseases, and immune-mediated disorders and other diseases in humans.[24,25]

Studies have revealed the important roles of phospholipids and phosphoinositides in various stages of autophagy, and PLD-derived PA suppresses autophagy.[26] Interestingly, studies indicate that mammalian PLD1 serves as both a positive and a negative regulator of autophagy in mammalian cells; however, how phosphoinositides and PLD are differentially involved in autophagy and autophagic flux regulation to modulate development remains largely unknown in plants. Here, we showed that PLDζ2 promotes the acidification of the vacuolar lumen by interacting with V-ATPase subunit D (VATD) under phosphorus deficiency, leading to the enhanced degradation of the autophagic body in vacuoles and improved plant adaption to phosphorus starvation.

## RESULTS

### Defective autophagic flux in *pldζ2* mutant

Our previous study showed that PLD-deficient mutants *pldα1*, *pldζ1*, *pldβ1*, and *pldδ* promoted autophagy, as reflected by the delayed yellowing of seedlings and increased chlorophyll contents upon nutrient starvation, while the PLDδ-overexpressing (*PLDδ-OE*) line was more sensitive to nutrient starvation.[26] Interestingly, different from the above PLD-deficient mutants, observations of seedling growth showed that both *pldζ2* and *PLDζ2-OE* plants were more sensitive to carbon or nitrogen starvation (Figures 1A and 1B) and displayed premature leaf senescence (Figure S1), which suggested the distinct function and regulatory mechanism of PLDζ2 in autophagy.

To investigate the role of PLDζ2 in autophagy, we examined the transcription of *ATG* genes, including *ATG2*, *ATG5*, *ATG6*, *ATG7*, *ATG8a*, *ATG8e*, *ATG9*, *ATG10*, *ATG18a*, *VPS34*, and *NBR1*, and found that they all were notably increased in the *pldζ2* mutant, and most of them (except for *ATG5*, *ATG7*, and *NBR1*) were significantly reduced in *PLDζ2-OE* plants (Figure S2). *Arabidopsis* seedlings expressing the GFP-ATG8e fusion protein were used widely as a marker for identifying autophagic structures, and by crossing the *pldζ2* and *PLDζ2-OE* seedlings with those expressing GFP-ATG8e, we observed that that compared to wild-type (WT) root cells, there were more GFP-ATG8e-labeled dots and ring-like structures in *pldζ2* and many fewer in *PLDζ2-OE* plants (Figure 1C). Further transmission electron microscopy (TEM) analysis of leaves' ultrastructure revealed increased autophagy-related structures, including chlorophagy and mitophagy in *pldζ2*, and decreased structures in *PLDζ2-OE* plants compared to the WT (Figures 1D and S3). Compared to the significantly reduced autophagy-related structures (~70% of the WT) in *PLDδ-OE*, the autophagic activity of *PLDζ2-OE* presented less of a decrease (by nearly 50%), suggesting that PLDζ2 regulates autophagy differently from other PLDs.[26]

The accumulation of autophagic structures, combined with suppressed autophagy as indicated by premature leaf senescence and reduced chlorophyll content during nutrient starvation, suggests that the autophagic flux may be defective in *pldζ2*. Indeed, immunoblotting analysis of the formation of ATG8-PE conjugates, which is necessary for autophagosome biogenesis, showed increased ATG8-PE in *pldζ2* upon carbon or nitrogen starvation (Figure 1E), demonstrating the increased autophagosomes in *pldζ2*. NBR1 serves as a link between ATG8 and ubiquitinated substrates and is efficiently degraded by autophagy; thus, the NBR1 protein level was used to monitor the autophagic flux, and deficiency of the *ATG7* gene led to increased NBR1 levels.[21,23,27] Further analysis showed that both the transcription and protein levels of NBR1 were dramatically increased in *pldζ2* (Figures 1F and S2), confirming the defective autophagic flux under *PLDζ2* deficiency.

Autophagy is a protective mechanism that is essential for the disposal of damaged organelles and the maintenance of cellular reactive oxygen species (ROS) homeostasis in plants.[28–30] Being consistent with more GFP-ATG8e-labeled dots and ring-like structures in *pldζ2* and many fewer in *PLDζ2-OE* plants (Figure 1C), observations of 7-day-old *pldζ2* and *PLDζ2-OE* roots stained with diaminobenzidine (DAB), nitroblue tetrazolium (NBT), and 2′,7′-dichlorofluorescin diacetate (DCFH-DA) showed the pronounced accumulation of $H_2O_2$, superoxide anion, and ROS in *pldζ2* roots (Figure S4), further demonstrating the defective autophagic flux in *pldζ2*.

### Impaired vacuole morphology and degradation under PLDζ2 deficiency

Blocked autophagic flux indicates a disruption in the dynamic process of autophagy, which can occur at various stages, including autophagosome formation, transport, fusion with vacuoles, or degradation within vacuoles. Considering that the autophagosome fuses with vacuoles to release the autophagic body, the lytic vacuole morphology and lytic degradation in *pldζ2* were analyzed. By labeling vacuoles with FM4-64 or LysoTracker, staining with 2',7'-Bis-(2-Carboxyethyl)-5-(and-6)-Carboxyfluorescein (BCECF), or observing the localization of tonoplast marker VAMP711-GFP, results showed the dramatic morphological abnormalities of *pldζ2* vacuoles that involved ectopic endomembrane inclusions into the vacuolar lumen, i.e., an unusual abundance of membrane budding (Figure 2A), which is consistent with the previous study and indicates that the degradation capacity of vacuoles may decrease in *pldζ2*, leading to the

(D) TEM analysis (left, bars: 50 μm) and quantification of autophagic structures (right) in WT, *pldζ2*, and *PLDζ2-OE* seedlings. Mesophyll cells of 3-week-old seedlings were observed. "A" indicates the autophagic structures. C, chloroplast; M, mitochondrion; V, vacuole. Experiments were biologically repeated three times, and data are mean ± SD (10 cells per seedling). Statistical significance was determined by Student's t test (*$p < 0.05$ and **$p < 0.01$; compared to WT).
(E) ATG8 lipidation detection of WT, *pldζ2*, and *PLDζ2-OE* seedlings upon carbon or nitrogen starvation. Five-day-old seedlings were incubated in MS liquid medium with or without carbon or nitrogen starvation. Crude extracts were subjected to ultracentrifuge to collect the membrane fractions of cells, followed by immunoblotting with anti-ATG8 antibody. Anti-actin antibody was used to examine the loading of proteins.
(F) Analysis of autophagic flux of WT, *pldζ2*, *atg7*, and *PLDζ2-OE* seedlings upon carbon or nitrogen starvation by immunoblotting using anti-NBR1 antibody. Experiments were biologically repeated, and anti-actin antibody was used to examine the loading of proteins.

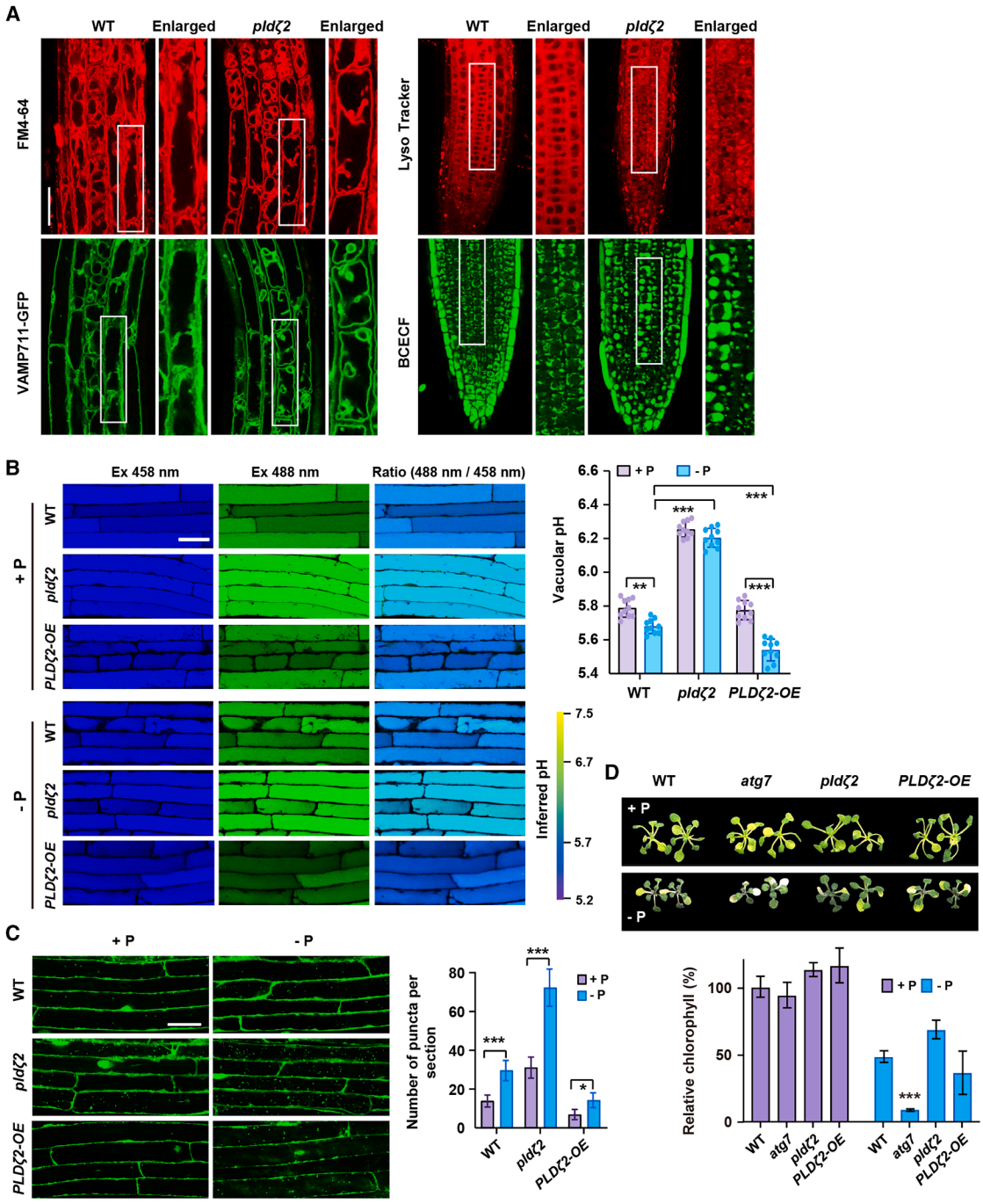


**Figure 2. Lytic vacuole morphology and lytic degradation are impaired in *pldζ2* mutant**

(A) Five-day-old WT and *pldζ2* seedlings were stained with FM4-64, BCECF, and LysoTracker and visualized by fluorescence confocal microscopy. Subcellular localization of vacuolar marker VAMP711-GFP in epidermal cells was observed. Bar: 50 μm.

(B) Emission intensities of epidermal root cell vacuoles (left, bar: 50 μm) and measurement (right) of vacuolar pH of WT, *pldζ2*, and *PLDζ2-OE* seedlings upon phosphorus starvation. Five-day-old seedlings were stained with BCECF-AM and visualized by fluorescence confocal microscopy. Under phosphorus starvation, the vacuolar pH of WT was reduced, while it was enhanced under PLDζ2 overexpression. Error bars represent SD of 10 measurements from 10 seedlings. Statistical significance was determined by Student's t test (**$p < 0.01$ and ***$p < 0.001$; compared to control).

(C) Observation of GFP-ATG8e-labeled dots and ring-like structures (left, bar: 50 μm) and calculation of puncta numbers per root section (right) upon phosphorus starvation. Seedlings expressing GFP-ATG8e fusion protein were grown on 1/2 MS medium for 5 days and then transferred to 1/2 MS medium with or without phosphorus and visualized by confocal microscopy. Experiments were biologically repeated three times, and data are mean ± SD ($n = 15$). Statistical significance was determined by Student's t test (*$p < 0.05$ and ***$p < 0.001$).

*(legend continued on next page)*

accumulated membranous structures in vacuoles.[31] The degradation capacity of vacuoles is largely affected by acidification status, and further measurement of root elongation zone cells using the dual-excitation ratiometric pH indicator BCECF acetoxymethyl ester (BCECF-AM) showed the significantly increased vacuolar pH in *pldζ2* compared to the WT (Figure 2B), indicating the reduced vacuolar acidification of *pldζ2*, which is consistent with the impaired autophagic flux and accumulated autophagic structures.[32]

*PLDζ2* transcription is specifically upregulated by phosphorus starvation, and our analysis further revealed the significantly increased transcription of *PLDζ2* upon carbon and nitrogen starvation as well (Figure S5).[33] In addition to the studies showing that PLDζ2-mediated PA promoted lateral root elongation and root hair development under low-phosphorus conditions through auxin signaling, observations using confocal microscopy indicated that the GFP-ATG8e-labeled dots and ring-like structures were significantly accumulated in *pldζ2*, while decreased in *PLDζ2-OE* plants, under phosphorus starvation (Figure 2C).[33,34] Phenotypic analysis showed that there was no significant growth difference of *pldζ2* and *PLDζ2-OE* seedlings upon phosphorus starvation (*atg7* was more sensitive; Figure 2D), which might due to the accumulation of anthocyanins caused by phosphorus starvation.[35–37] However, *pldζ2* and *PLDζ2-OE* seedlings were more sensitive to both nitrogen and phosphorus starvation (Figure S6, top). Compared with that upon nitrogen starvation (Figure 1B), there was more of a decrease in chlorophyll content upon nitrogen and phosphorus starvation (Figure S6, bottom), indicating the involvement and importance of autophagy in nutrients, particularly phosphorus starvation. Compared to the reduced vacuolar pH (increased vacuolar acidification) of the WT under phosphorus starvation, *pldζ2* presented no change, while *PLDζ2-OE* plants presented much lower vacuolar pH (Figure 2B), demonstrating the crucial role of PLDζ2 in response to phosphorus starvation by stimulating vacuolar acidification and autophagy.

## PLDζ2 interacts with V-ATPase subunit VATD

To investigate the functional mechanism of PLDζ2 in regulating vacuolar pH, seedlings expressing PLDζ2-GFP were counterstained with propidium iodide (PI) and then visualized by fluorescence confocal microscopy. Results showed that PLDζ2-GFP was localized to punctate structures, cytoplasmic space, and the tonoplast under normal growth conditions (Figures 3A and S7), which is consistent with previous studies showing the tonoplast localization of PLDζ2.[31,38] Further observations showed that the punctate structures of PLDζ2 (mainly the multivesicular body) decrease, while its cytoplasmic and tonoplast localization increases under phosphate starvation (Figures 3A and S7), suggesting that phosphorus deficiency reduces PLDζ2 targeting to multivesicular bodies but significantly enhances its localization at the tonoplast. In addition, observation of *N. benthamiana* leaves transiently co-expressing PLDζ2-GFP with Histidine-Aspartic acid-Glutamic acid-Leucine (HDEL)-mCherry showed that PLDζ2 also localizes at the endoplasmic reticulum (ER) (Figure 3B).

Autophagosomes are degraded in vacuoles by abundant hydrolytic enzymes in an acidic environment, which depends on the function of V-ATPase.[39] Besides the tonoplast-localized V-ATPases, the ATPase at the *trans*-Golgi network/early endosome (TGN/EE) also contributes to vacuolar acidification.[1,40] *Arabidopsis* PLDζ2 is localized to multiple compartments, including the TGN, multivesicular bodies, and the tonoplast, while PLDζ1 is found in the TGN.[38] To determine whether tonoplast-localized or TGN-localized PLDζ2 regulates vacuolar acidification, the vacuolar pH of *pldζ1* mutant was measured. Compared to the WT, there is no significant change of *pldζ1* under normal conditions or phosphorus starvation (Figure S8), suggesting that tonoplast-localized PLDζ2 regulates vacuolar acidification under phosphorus starvation.

To search for the PLDζ2-associated tonoplast components, yeast two-hybrid (Y2H) analysis was performed, and VATD was detected to specifically interact with PLDζ2 (Figure S9). A bimolecular fluorescence complementation (BiFC) study co-expressing nYFP-PLDζ2 and VATD-cYFP in *N. benthamiana* leaves showed detectable YFP fluorescence (Figure 3C). Co-immunoprecipitation (coIP) analysis further demonstrated the interaction of PLDζ2-GFP with VATD-mCherry *in vivo* (Figure 3D). Fluorescence resonance energy transfer with fluorescence lifetime imaging microscopy (FRET-FLIM) has become a common technique for studying the conformational changes of biomolecules and dynamic interactions, and analysis by FRET-FLIM revealed a reduced fluorescence lifetime of PLDζ2-GFP when co-expressing VATD-mCherry (Figure 3E), confirming the PLDζ2-VATD interaction *in vivo*.[41]

## PLDζ2 promotes vacuolar acidification by interacting with VATD

Monodansylcadaverine (MDC), a fluorescent dye that preferentially accumulates in acidic lytic vacuoles, is commonly used as a marker to visualize vacuolar structures involved in autophagy.[42] To assess the VATD role in autophagy, 5-day-old WT and *vatd* mutant seedlings were treated with Concanamycin A (Con A) and then stained with MDC. Observation of autophagosomes using confocal microscopy showed that MDC-stained vesicles were significantly accumulated in vatd root cells (Figure 4A). Further analysis using TEM revealed increased autophagy-related structures in *vatd* leaves (Figure 4B), which is consistent with the *vatd* mutant being more sensitive to carbon and nitrogen starvation than the WT (Figure S10A), confirming the positive role of VATD in autophagy. Considering VATD is a subunit of V-ATPase, the vacuolar pH of *vatd* cells at the root elongation zone was measured using BCECF-AM, and the results showed the significantly increased vacuolar pH of *vatd*

(D) Phenotypic observation (left) and measurement of chlorophyll contents of WT, *pldζ2* and *atg7* mutants, and *PLDζ2-OE* seedlings upon phosphorus starvation. Seedlings were grown on MS medium for 1 week and then transferred to MS medium with or without phosphorus under normal growth conditions. Relative chlorophyll contents were calculated by comparing the values of –P seedlings to those of +P conditions (right). Experiments were biologically repeated three times, and data are mean ± SD ($n$ = 15). Statistical significance was determined by Student's t test (***$p < 0.001$; compared to WT at same condition).

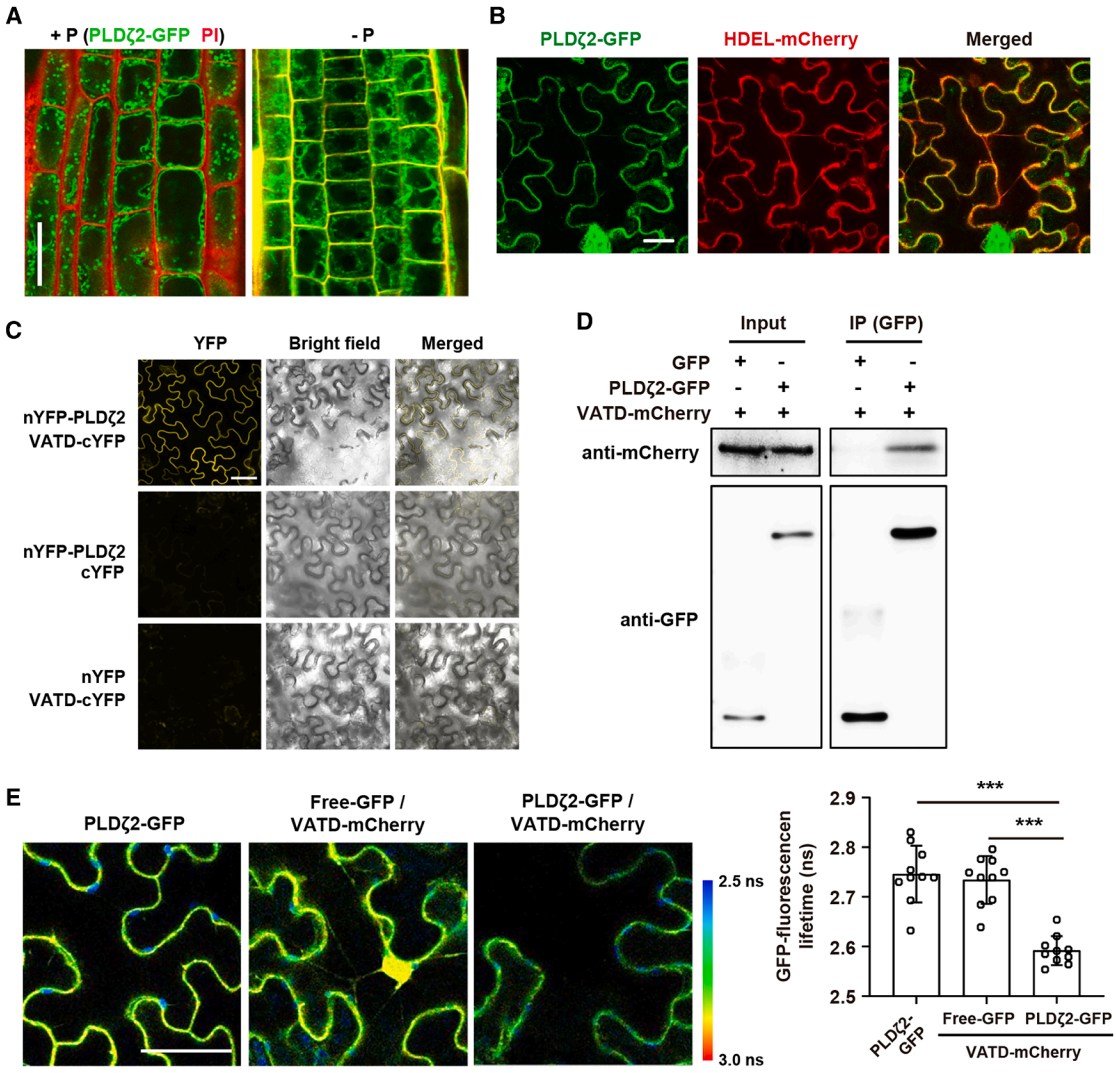


**Figure 3. PLDζ2 locates at tonoplast and interacts with V-ATPase VATD**

(A) Five-day-old *Arabidopsis* seedlings expressing PLDζ2-GFP were counterstained with propidium iodide (PI) and visualized by fluorescence confocal microscopy. Experiments were conducted under both normal and phosphorus-deficient conditions. Representative images are shown (bar: 50 μm).

(B) Observation of *N. benthamiana* leaves co-expressing PLDζ2-GFP with ER marker HDEL-mCherry. Representative images are shown (bar: 50 μm).

(C) BiFC analysis using *N. benthamiana* leaf epidermal cells showed the interaction between PLDζ2 and VATD. Bar: 50 μm.

(D) Co-immunoprecipitation (coIP) assay demonstrated the interaction between VATD-mCherry and PLDζ2-GFP *in vivo*. GFP-tagged PLDζ2 was transiently co-expressed with mCherry-VATD in *Arabidopsis* protoplasts and immunoprecipitated by GFP affinity magnetic beads. Resultant immunoprecipitation and cell lysates were analyzed by immunoblotting using anti-GFP or anti-mCherry antibodies.

(E) FRET-FLIM analysis (top) and quantification of fluorescence lifetime (bottom) of PLDζ2-GFP expressed alone or co-expressed with VATD-mCherry in *N. benthamiana*. Representative images are shown (bar: 50 μm). Data are mean ± SD ($n$ = 10). An ANOVA followed by Tukey test revealed the significant differences (***$p < 0.001$).

under normal growth conditions (Figure 4C), which is consistent with the suppressed autophagy of *vatd*. In addition, compared to the reduced vacuolar pH (increased vacuolar acidification) under phosphorus starvation of the WT, *vatd* presented no change of vacuolar pH compared to the normal condition (Figure 4C), which is consistent with *vatd* being more sensitive to phosphorus starvation (Figure 4D) or carbon and phosphorus starvation (Figure S10B), confirming the role of VATD in nutrient starvation—promoting autophagy by regulating vacuolar pH.

Compared to that of the WT, the vacuolar pH of *vatd/PLDζ2-OE* was significantly increased, while there was no change of *pldζ2/VATD-OE* under normal growth conditions. There is a reduced vacuolar pH (increased vacuolar acidification) of the WT under phosphorus starvation; however, the *vatd/PLDζ2-OE* seedlings showed no change, while *pldζ2/VATD-OE* seedlings presented much lower vacuolar pH (Figure 4C), indicating that PLDζ2 functions upstream of VATD to promote the vacuolar acidification under phosphorus starvation.

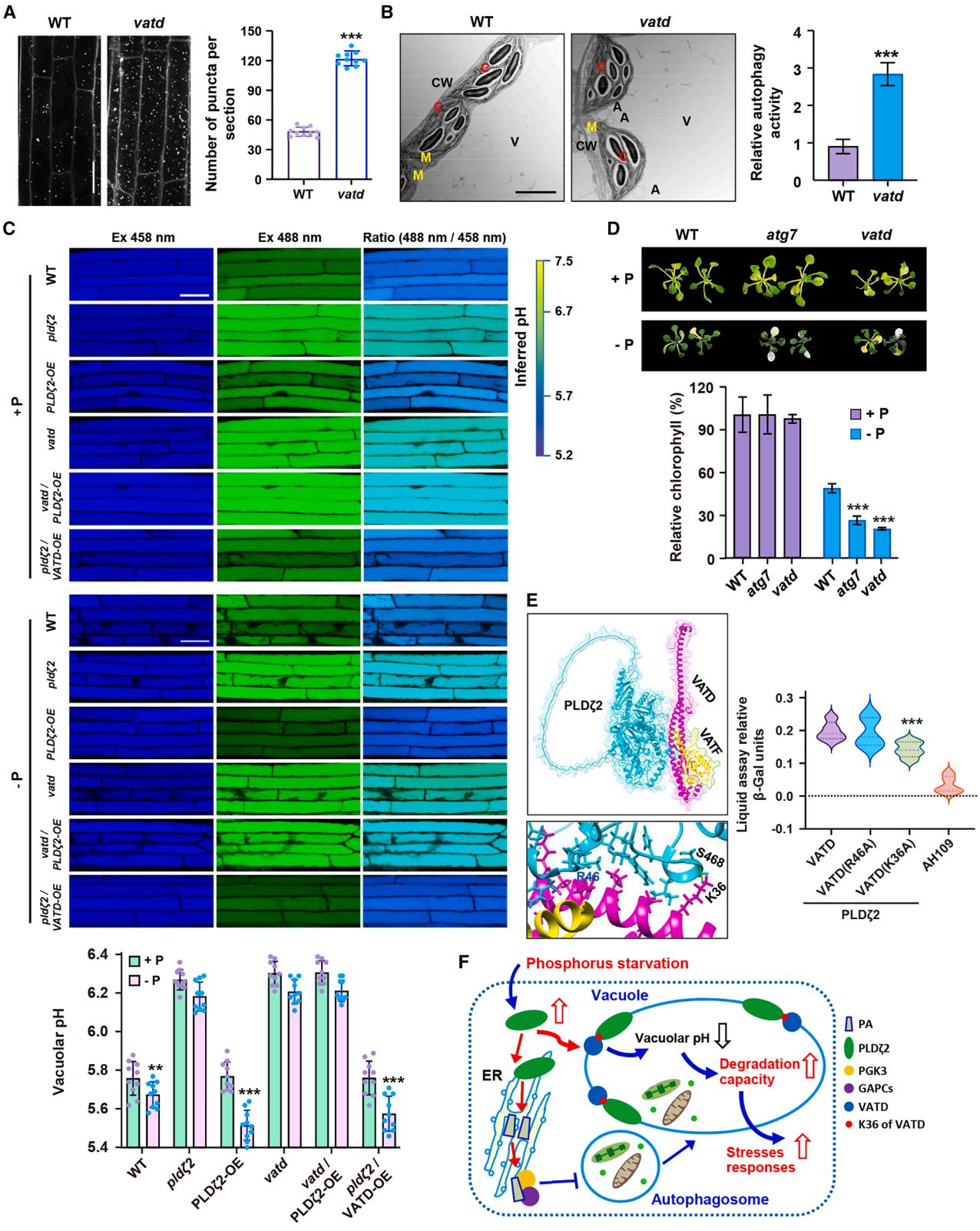


*(legend on next page)*

To demonstrate that the interaction between PLDζ2 and VATD is required for promoted vacuolar acidification, AlphaFold was applied to analyze the conservation of the overall structure of individual subunits and their respective binding interface. Due to V-ATPase subunits D and F forming a central rotor axle of V-ATPase, the binding interfaces of the module composed of PLDζ2-VATD-VATF were predicted. Analyses of the amino acids involved in the formation of hydrogen bonds revealed that PLDζ2 is linked to VATD via serine (S) 468 in PLDζ2 and lysine (K)36 in VATD (Figure 4E, left). Indeed, the β-galactosidase (β-gal) liquid assay using mutated VATD (K36 is substituted with A; R46, which does not affect the PLDζ2-VATD interaction, is substituted with A and used as a control) showed that the PLDζ2-VATD interaction substantially decreased (Figure 4E, right) compared to normal VATD, confirming the crucial role of K36 of VATD in PLDζ2-VATD interactions.

## DISCUSSION

We demonstrated that PLDζ2 facilitates the vacuolar acidification and degradation of autophagic bodies in response to phosphorus and nutrient starvation by directly interacting with VATD, which supports a mechanistic model of how PLDζ2 coordinates vacuolar acidification and autophagy in plants. Under phosphorus starvation, the transcription of *PLDζ2* was rapidly upregulated, and increased PLDζ2 located at the tonoplast facilitates vacuolar acidification by interacting with VATD protein, hence promoting autophagy in response to phosphorus starvation; on the other hand, increased PLDζ2 stimulates the PA production at the ER to suppress autophagy by binding glyceraldehyde-3-phosphate dehydrogenases (GAPCs) and phosphoglycerate kinase 3 (PGK3) proteins (Figure 4F).[26] Our study elucidates the molecular mechanism of how plants maintain cellular homeostasis through different locations of PLDζ2 and expands the understanding of the regulatory mechanism of autophagy by vacuolar acidification in plants, providing a new perspective for autophagy regulation.

Vacuolar acidification, the process of increasing the concentration of $H^+$ ions in vacuoles, is fundamental to maintaining the acidic environment and cellular homeostasis, enabling nutrient storage, promoting growth, and enhancing the plant's ability to adapt to biotic and abiotic challenges.[43] Regulation of vacuolar acidification is a key aspect of plant physiology, and our results revealed that PLDζ2 interacts with VATD to promote vacuolar acidification under phosphorus starvation, providing a possible molecular mechanism for crops to maintain vacuolar acidity and cellular homeostasis under nutrient starvation. It is noticed that the vacuolar pH in the *pldζ2* mutant was higher under phosphorus-sufficient conditions, which suggests that the PLDζ2-VATD interaction also contributes to maintaining vacuolar acidity during normal growth, highlighting a broader physiological role of PLDζ2 in vacuolar pH homeostasis beside the phosphorus-starvation responses.

In addition, the lipid composition of the endomembrane is crucial for regulating V-ATPase activity. In yeast, elevated levels of the signaling lipid phosphatidylinositol-3,5-bisphosphate (PI(3,5)$P_2$) enhance V-ATPase assembly, thereby increasing its activity.[13] Similarly, PI(3,5)$P_2$ has been observed to facilitate vacuolar lumen acidification during abscisic acid (ABA)-induced stomatal closure in plants.[44,45] In this study, we focus on the function of PLDζ2, and the effect of PA produced by PLDζ2 on V-ATPase activity requires further investigations. Considering that most studies on PLD focus on analyzing the target proteins of PA generated by PLD hydrolysis, our studies open up a new perspective for PLD function in regulating various biological processes.

**Figure 4. PLDζ2 interacts with VATD to regulate vacuolar pH**

(A) MDC staining (left) and quantification of puncta number per root section (right) of WT and *vatd* mutant. Five-day-old seedlings were treated with 0.5 μM Con A, followed by staining with MDC. The labeled autophagosomes were visualized by fluorescence confocal microscopy using a DAPI-specific filter, and representative images are shown (bar: 50 μm). Numbers of puncta per root section are presented as mean ± SD ($n$ = 10). Statistical significance was determined by Student's t test (***$p < 0.001$; compared to WT).

(B) TEM analysis (left) and quantification of autophagic structures (right) in WT and *vatd* mutant. Three-week-old seedlings were treated with Con A (0.5 μM), and mesophyll cells were observed. Representative images are shown (bar: 50 μm). "A" indicates the autophagic structures. CW, cell wall; C, chloroplast; M, mitochondrion; V, vacuole. Experiments were biologically repeated three times, and data are mean ± SD (10 cells per seedling). Statistical significance was determined by Student's t test (***$p < 0.001$; compared to WT).

(C) Emission intensities of epidermal root cell vacuoles (left, bar: 50 μm) and measurement (right) of vacuolar pH of WT, *vatd*, *pldζ2*, *PLDζ2-OE*, *pldζ2/VATD-OE*, and *vatd/PLDζ2-OE* upon phosphorus starvation. Five-day-old seedlings were stained with BCECF-AM and visualized by fluorescence confocal microscopy. Error bars represent SD of 10 measurements from 10 seedlings. Statistical significance was determined by Student's t test (**$p < 0.01$ and ***$p < 0.001$; compared to control).

(D) Phenotypic observation (top) and measurement of chlorophyll contents of WT and *atg7* and *vatd* mutants upon phosphorus starvation. Seedlings were grown on MS medium for 1 week and then transferred to MS medium with or without phosphorus under normal growth conditions. Relative chlorophyll contents were calculated by comparing the values of –P seedlings to those of +P conditions (bottom). Experiments were biologically repeated three times, and data are mean ± SD ($n$ = 15). Statistical significance was determined by Student's t test (***$p < 0.001$; compared to WT at same condition).

(E) Structural diagram of the PLDζ2-VATD-VATF complex was calculated by a hybrid docking approach using AlphaFold. Proteins are shown in the cartoon and surface model, with PLDζ2 colored in cyan, VATD in pink, and VATF in yellow (top left). In the zoom graph (bottom left), the amino acids of PLDζ2 that could establish hydrogen bonds (indicated by green lines) with VATD are predicted based on the docking model. Y2H β-galactosidase liquid assays (right) were performed using PLDζ2 with normal VATD or mutated VATD ($VATD^{R46A}$ or $VATD^{K36A}$), and interaction values were normalized to that of AH109. Statistical significance was determined by Student's t test (***$p < 0.001$; compared to normal VATD).

(F) A hypothetical model illustrating how PLDζ2 finely regulates vacuolar acidification and autophagy in *Arabidopsis*. Under nutrient starvation, especially phosphorus starvation, PLDζ2 is rapidly induced and localizes to the tonoplast, where it interacts with VATD to facilitate vacuolar acidification, leading to an increase in the degradation capacity of vacuoles, thus promoting autophagic body degradation to response to nutrient deficiency. On the other hand, PLDζ2 located in the ER catalyzes the hydrolysis of structural phospholipids to produce phosphatidic acid (PA), which suppresses autophagy through competitive inhibition by binding to GAPCs and PGK3 proteins.

In mammalian cells, depletion of PLD1 significantly promotes the autophagic process in HEK293 and HeLa cells under prolonged starvation, whereas knockdown or chemical inhibition of PLD1 in mouse cells decreases the number of autophagosomes under nutrient starvation.[46,47] In *Arabidopsis*, PLDε has been found to promote autophagy by interacting with ATG8 under nitrogen deficiency.[48] Our previous study showed that PLD-deficient mutants (pldα1, pldζ1, pldβ1, and pldδ) present enhanced autophagy under nutrient-starvation conditions.[26] We here demonstrated that PLDζ2 stimulates autophagic degradation under phosphorus deficiency by promoting the acidification of the vacuolar lumen. Nutrient deficiencies, particularly phosphorus deficiency, induce PLDζ2 expression and promote cell autophagy to enhance cell tolerance to starvation stress. However, PLDζ2 overexpression exhibits the opposite phenotype, which may be due to ER-localized PLDζ2 stimulating PA production to suppress autophagy by binding to GAPCs and PGK3 proteins.[26] Considering the conservation of PLD and autophagy, our studies reveal the differential effects of PLDζ2 on plant autophagy in different locations, which provide clues for elucidating the dual role of mammalian PLD1 in autophagy in response to starvation. In addition, regarding the relatively conserved functions and regulatory mechanism of VATD in the lysosome of mammals and vacuoles of plant cells, the finding that VATD interacts with PLDζ2 to facilitate vacuolar acidification will help to clarify the mechanism of how lysosomal pH and the acidic environment, as well as the cellular homeostasis, of mammals is maintained.

During the process of autophagy, the double-membraned autophagosome fuses with the lysosome and vacuole membranes, entering the lysosome or central vacuole, where hydrolases break down their contents in an acidified environment regulated by V-ATPase activity.[49,50] When bacterial infection causes vacuolar damage, V-ATPase recruits ATG16L1 to the bacteria-containing vacuole, initiating the autophagic response following bacteria-induced vacuolar damage, while SopF inhibits this process by blocking the interaction between V-ATPase and ATG16L1.[51] The replicase γa of the Barley stripe mosaic virus directly prevents the acidification of the vacuolar lumen and inhibits autophagic degradation, thereby enhancing viral infection in plants.[39] These studies demonstrate the close relationship between vacuolar acidification and autophagy. Our study revealed that PLDζ2 promotes vacuolar acidification and degradation of autophagic bodies in response to phosphorus deficiency by directly interacting with VATD, providing informative clues for elucidating the mechanism of autophagy regulation under nutrient starvation.

### Limitations of the study

While this study provides significant insights into the role of PLDζ2 in promoting vacuolar acidification and autophagic degradation under nutrient deficiency, several limitations should be acknowledged. First, the findings were primarily based on *Arabidopsis*, and it remains unclear whether similar mechanisms are conserved across other plant species or in different environmental contexts. Second, although genetic, structural, and biochemical approaches were used to demonstrate the interaction between PLDζ2 and VATD, additional studies are needed to determine the dynamic regulation and structural basis of this interaction under varying nutrient conditions. Future research should aim to address these gaps by investigating cross-species conservation and the detailed molecular mechanisms underlying PLDζ2-mediated regulation.

## RESOURCE AVAILABILITY

### Lead contact

Further information and requests for resources and reagents should be directed to and will be fulfilled by the lead contact, Hong-Wei Xue (hwxue@sjtu.edu.cn).

### Materials availability

Materials newly produced in this work are available from the lead contact upon reasonable request.

### Data and code availability

- No data from this study have been deposited in external repositories. However, the sequence data for *Arabidopsis* genes examined in this work are accessible via The Arabidopsis Information Resource (www.arabidopsis.org) under the following accession numbers: *PLDζ1*, AT3G16785; *PLDζ2*, AT3G05630; *VATD*, AT3G58730; *PLDα1*, AT3G15730; *PLDβ1*, AT2G42010; *PLDδ1*, AT4G35790; *ATG2*, AT4G35790; *ATG5*, AT5G17290; *ATG6*, AT3G61710; *ATG7*, AT5G45900; *ATG8a*, AT4G21980; *ATG8e*, AT2G45170; *ATG9*, AT2G31260; *ATG10*, AT3G07525; *ATG18a*, AT3G62770; *VPS34*, AT3G62770; and *NBR1*, AT3G62770.
- This study does not report original code.
- Any additional information required to reanalyze the data reported in this paper is available from the lead contact upon request.

## ACKNOWLEDGMENTS

The study was supported by National Natural Science Foundation of China (NSFC, 92354301, 32230011, 32200274, and 91954206). The computations were run on the Siyuan-1 cluster supported by the Center for High-Performance Computing at Shanghai Jiao Tong University.

## AUTHOR CONTRIBUTIONS

B.G. and H.-W.X. conceived and designed the experiments. B.G. performed the experiments and drafted the manuscript. K.-X.X., X.-Q.D., and P.-C.H. helped to generate transgenic lines and observe the plant growth. Y.-X.B. helped to analyze the protein structure and interactions. W.-H.L. and J.F. discussed the results. H.-W.X. wrote the paper.

## DECLARATION OF INTERESTS

The authors declare no competing interests.

## STAR★METHODS

Detailed methods are provided in the online version of this paper and include the following:

- KEY RESOURCES TABLE
- EXPERIMENTAL MODEL AND STUDY PARTICIPANT DETAILS
  - Plant materials, growth condition, and treatments
- METHOD DETAILS
  - Constructs
  - Measurement of chlorophyll contents
  - Detection of autophagy
  - Transmission electron microscopy (TEM) analysis
  - Protein extraction and western blotting analysis
  - Yeast two-hybrid (Y2H), Bimolecular Fluorescent Complimentary (BiFC) and subcellular localization analysis
  - Co-immunoprecipitation (Co-IP) analysis

- Fluorescence resonance energy transfer with fluorescence lifetime imaging microscopy (FRET-FLIM) assays
- Molecular modeling

- QUANTIFICATION AND STATISTICAL ANALYSIS

## SUPPLEMENTAL INFORMATION

Supplemental information can be found online at https://doi.org/10.1016/j.celrep.2025.116024.

Received: January 6, 2025
Revised: April 4, 2025
Accepted: June 27, 2025

## REFERENCES

1. Holzheu, P., Krebs, M., Larasati, C., Schumacher, K., and Kummer, U. (2021). An integrative view on vacuolar pH homeostasis in *Arabidopsis thaliana*: Combining mathematical modeling and experimentation. Plant J. *106*, 1541–1556.
2. Ungermann, C., Wickner, W., and Xu, Z. (1999). Vacuole acidification is required for trans-SNARE pairing, LMA1 release, and homotypic fusion. Proc. Natl. Acad. Sci. USA *96*, 11194–11199.
3. Cui, Y., Zhao, Q., Hu, S., and Jiang, L. (2020). Vacuole biogenesis in plants: how many vacuoles, how many models? Trends Plant Sci. *25*, 538–548.
4. Zhang, C., Hicks, G.R., and Raikhel, N.V. (2014). Plant vacuole morphology and vacuolar trafficking. Front. Plant Sci. *5*, 476.
5. Futai, M., Sun-Wada, G.H., Wada, Y., Matsumoto, N., and Nakanishi-Matsui, M. (2019). Vacuolar-type ATPase: A proton pump to lysosomal trafficking. Proc. Jpn. Acad. *95*, 261–277.
6. Vasanthakumar, T., and Rubinstein, J.L. (2020). Structure and roles of V-type ATPases. Trends Biochem. Sci. *45*, 295–307.
7. Birgisdottir, Å.B., and Johansen, T. (2020). Autophagy and endocytosis - interconnections and interdependencies. J. Cell Sci. *133*, 228114.
8. Collins, M.P., and Forgac, M. (2020). Regulation and function of V-ATPases in physiology and disease. Biochim. Biophys. Acta. Biomembr. *1862*, 183341.
9. Song, Q., Meng, B., Xu, H., and Mao, Z. (2020). The emerging roles of vacuolar-type ATPase-dependent lysosomal acidification in neurodegenerative diseases. Transl. Neurodegener. *9*, 17.
10. Sze, H., Schumacher, K., Müller, M.L., Padmanaban, S., and Taiz, L. (2002). A simple nomenclature for a complex proton pump: VHA genes encode the vacuolar $H^+$-ATPase. Trends Plant Sci. *7*, 157–161.
11. Banerjee, S., and Kane, P.M. (2017). Direct interaction of the Golgi V-ATPase a-subunit isoform with PI(4)P drives localization of Golgi V-ATPases in yeast. Mol. Biol. Cell *28*, 2518–2530.
12. Banerjee, S., Clapp, K., Tarsio, M., and Kane, P.M. (2019). Interaction of the late endo-lysosomal lipid $PI(3,5)P_2$ with the Vph1 isoform of yeast V-ATPase increases its activity and cellular stress tolerance. J. Biol. Chem. *294*, 9161–9171.
13. Banerjee, S., and Kane, P.M. (2020). Regulation of V-ATPase activity and organelle pH by phosphatidylinositol phosphate lipids. Front. Cell Dev. Biol. *8*, 510.
14. Mitra, C., Winkley, S., and Kane, P.M. (2023). Human V-ATPase a-subunit isoforms bind specifically to distinct phosphoinositide phospholipids. J. Biol. Chem. *299*, 105473.
15. Testerink, C., Dekker, H.L., Lim, Z.Y., Johns, M.K., Holmes, A.B., Koster, C.G., Ktistakis, N.T., and Munnik, T. (2004). Isolation and identification of phosphatidic acid targets from plants. Plant J. *39*, 527–536.
16. Yao, H.Y., and Xue, H.W. (2018). Phosphatidic acid plays key roles regulating plant development and stress responses. J. Integr. Plant Biol. *60*, 851–863.
17. Li, G., and Xue, H.W. (2007). *Arabidopsis* PLDζ2 regulates vesicle trafficking and is required for auxin response. Plant Cell *19*, 281–295.
18. Cruz-Ramírez, A., Oropeza-Aburto, A., Razo-Hernández, F., Ramírez-Chávez, E., and Herrera-Estrella, L. (2006). Phospholipase DZ2 plays an important role in extraplastidic galactolipid biosynthesis and phosphate recycling in *Arabidopsis* roots. Proc. Natl. Acad. Sci. USA *103*, 6765–6770.
19. Michaeli, S., Galili, G., Genschik, P., Fernie, A.R., and Avin-Wittenberg, T. (2016). Autophagy in plants–what's new on the menu? Trends Plant Sci. *21*, 134–144.
20. Qi, H., Xia, F.N., and Xiao, S. (2021). Autophagy in plants: Physiological roles and post-translational regulation. J. Integr. Plant Biol. *63*, 161–179.
21. Doelling, J.H., Walker, J.M., Friedman, E.M., Thompson, A.R., and Vierstra, R.D. (2002). The APG8/12-activating enzyme APG7 is required for proper nutrient recycling and senescence in *Arabidopsis thaliana*. J. Biol. Chem. *277*, 33105–33114.
22. Minina, E.A., Sanchez-Vera, V., Moschou, P.N., Suarez, M.F., Sundberg, E., Weih, M., and Bozhkov, P.V. (2013). Autophagy mediates caloric restriction-induced lifespan extension in *Arabidopsis*. Aging Cell *12*, 327–329.
23. Xiong, Y., Contento, A.L., and Bassham, D.C. (2005). AtATG18a is required for the formation of autophagosomes during nutrient stress and senescence in *Arabidopsis thaliana*. Plant J. *42*, 535–546.
24. Klionsky, D.J., Abdel-Aziz, A.K., Abdelfatah, S., Abdellatif, M., Abdoli, A., Abel, S., Abeliovich, H., Abildgaard, M.H., Abudu, Y.P., Acevedo-Arozena, A., et al. (2021). Guidelines for the use and interpretation of assays for monitoring autophagy (4th edition). Autophagy *17*, 1–382.
25. Zhang, X.J., Chen, S., Huang, K.X., and Le, W.D. (2013). Why should autophagic flux be assessed? Acta Pharmacol. Sin. *34*, 595–599.
26. Guan, B., Jiang, Y.T., Lin, D.L., Lin, W.H., and Xue, H.W. (2022). Phosphatidic acid suppresses autophagy through competitive inhibition by binding GAPC (glyceraldehyde-3-phosphate dehydrogenase) and PGK (phosphoglycerate kinase) proteins. Autophagy *18*, 2656–2670.
27. Zhou, J., Wang, J., Cheng, Y., Chi, Y.J., Fan, B., Yu, J.Q., and Chen, Z. (2013). NBR1-mediated selective autophagy targets insoluble ubiquitinated protein aggregates in plant stress responses. PLoS Genet. *9*, e1003196.
28. Chen, L., Liao, B., Qi, H., Xie, L.J., Huang, L., Tan, W.J., Zhai, N., Yuan, L. B., Zhou, Y., Yu, L.J., et al. (2015). Autophagy contributes to regulation of the hypoxia response during submergence in *Arabidopsis thaliana*. Autophagy *11*, 2233–2246.
29. Guan, B., Lin, Z., Liu, D., Li, C., Zhou, Z., Mei, F., Li, J., and Deng, X. (2019). Effect of waterlogging-induced autophagy on programmed cell death in *Arabidopsis* roots. Front. Plant Sci. *10*, 468.
30. Yamauchi, S., Mano, S., Oikawa, K., Hikino, K., Teshima, K.M., Kimori, Y., Nishimura, M., Shimazaki, K.I., and Takemiya, A. (2019). Autophagy controls reactive oxygen species homeostasis in guard cells that is essential for stomatal opening. Proc. Natl. Acad. Sci. USA *116*, 19187–19192.
31. Yamaryo, Y., Dubots, E., Albrieux, C., Baldan, B., and Block, M.A. (2008). Phosphate availability affects the tonoplast localization of PLDζ2, an *Arabidopsis thaliana* phospholipase D. FEBS Lett. *582*, 685–690.
32. Krebs, M., Beyhl, D., Görlich, E., Al-Rasheid, K.A., Marten, I., Stierhof, Y. D., Hedrich, R., and Schumacher, K. (2010). *Arabidopsis* V-ATPase activity at the tonoplast is required for efficient nutrient storage but not for sodium accumulation. Proc. Natl. Acad. Sci. USA *107*, 3251–3256.
33. Lin, D.L., Yao, H.Y., Jia, L.H., Tan, J.F., Xu, Z.H., Zheng, W.M., and Xue, H. W. (2020). Phospholipase D - derived phosphatidic acid promotes root hair development under phosphorus deficiency by suppressing vacuolar degradation of PIN-FORMED2. New Phytol. *226*, 142–155.
34. Li, M., Qin, C., Welti, R., and Wang, X. (2006). Double knockouts of phospholipases Dζ1 and Dζ2 in *Arabidopsis* affect root elongation during phosphate-limited growth but do not affect root hair patterning. Plant Physiol. *140*, 761–770.
35. Jiang, C., Gao, X., Liao, L., Harberd, N.P., and Fu, X. (2007). Phosphate starvation root architecture and anthocyanin accumulation responses

are modulated by the gibberellin-DELLA signaling pathway in *Arabidopsis*. Plant Physiol. *145*, 1460–1470.

36. Zeliou, K., Kyzeridou, A., and Petropoulou, Y. (2022). Exposed red leaves display adaptive adjustments in chlorophyll and photosystem ratios compatible with the shade imposed by anthocyanin accumulation. Photosynthetica *60*, 70–78.
37. Wingler, A., Marès, M., and Pourtau, N. (2004). Spatial patterns and metabolic regulation of photosynthetic parameters during leaf senescence. New Phytol. *161*, 781–789.
38. Shimamura, R., Ohashi, Y., Taniguchi, Y.Y., Kato, M., Tsuge, T., and Aoyama, T. (2022). *Arabidopsis* PLDζ1 and PLDζ2 localize to post-Golgi membrane compartments in a partially overlapping manner. Plant Mol. Biol. *108*, 31–49.
39. Yang, M., Ismayil, A., Jiang, Z., Wang, Y., Zheng, X., Yan, L., Hong, Y., Li, D., and Liu, Y. (2022). A viral protein disrupts vacuolar acidification to facilitate virus infection in plants. EMBO J. *41*, e108713.
40. Farquharson, K.L. (2015). A TGN/EE-localized V-ATPase contributes to vacuolar acidification. Plant Cell *27*, 3292–3293.
41. Long, Y., Stahl, Y., Weidtkamp-Peters, S., Postma, M., Zhou, W., Goedhart, J., Sánchez-Pérez, M.I., Gadella, T.W.J., Simon, R., Scheres, B., and Blilou, I. (2017). In vivo FRET-FLIM reveals cell-type-specific protein interactions in *Arabidopsis* roots. Nature *548*, 97–102.
42. Contento, A.L., Xiong, Y., and Bassham, D.C. (2005). Visualization of autophagy in *Arabidopsis* using the fluorescent dye monodansylcadaverine and a GFP-AtATG8e fusion protein. Plant J. *42*, 598–608.
43. Kriegel, A., Andrés, Z., Medzihradszky, A., Krüger, F., Scholl, S., Delang, S., Patir-Nebioglu, M.G., Gute, G., Yang, H., Murphy, A.S., et al. (2015). Job sharing in the endomembrane system: vacuolar acidification requires the combined activity of V-ATPase and V-PPase. Plant Cell *27*, 3383–3396.
44. Li, S.C., Diakov, T.T., Xu, T., Tarsio, M., Zhu, W., Couoh-Cardel, S., Weisman, L.S., and Kane, P.M. (2014). The signaling lipid PI(3, 5)$P_2$ stabilizes V1–Vo sector interactions and activates the V-ATPase. Mol. Biol. Cell *25*, 1251–1262.
45. Bak, G., Lee, E.J., Lee, Y., Kato, M., Segami, S., Sze, H., Maeshima, M., Hwang, J.U., and Lee, Y. (2013). Rapid structural changes and acidification of guard cell vacuoles during stomatal closure require phosphatidylinositol 3, 5-bisphosphate. Plant Cell *25*, 2202–2216.
46. Jang, Y.H., Choi, K.Y., and Min, D.S. (2014). Phospholipase D - mediated autophagic regulation is a potential target for cancer therapy. Cell Death Differ. *21*, 533–546.
47. Dall'Armi, C., Hurtado-Lorenzo, A., Tian, H., Morel, E., Nezu, A., Chan, R. B., Yu, W.H., Robinson, K.S., Yeku, O., Small, S.A., et al. (2010). The phospholipase D1 pathway modulates macroautophagy. Nat. Commun. *1*, 142.
48. Yao, S., Peng, S., and Wang, X. (2022). Phospholipase Dε interacts with autophagy - related protein 8 and promotes autophagy in *Arabidopsis* response to nitrogen deficiency. Plant J. *109*, 1519–1534.
49. Marshansky, V., and Futai, M. (2008). The V-type H+-ATPase in vesicular trafficking: targeting, regulation and function. Curr. Opin. Cell Biol. *20*, 415–426.
50. Kissing, S., Saftig, P., and Haas, A. (2018). Vacuolar ATPase in phago (lyso) some biology. Int. J. Med. Microbiol. *308*, 58–67.
51. Xu, Y., Zhou, P., Cheng, S., Lu, Q., Nowak, K., Hopp, A.K., Li, L., Shi, X., Zhou, Z., Gao, W., et al. (2019). A bacterial effector reveals the V-ATPase-ATG16L1 axis that initiates xenophagy. Cell *178*, 552–566.e20.
52. Evans, R., O'Neill, M., Pritzel, A., Antropova, N., Senior, A., Green, T., Žídek, A., Bates, R., Blackwell, S., Yim, J., et al. (2021). Protein complex prediction with AlphaFold-Multimer. Preprint at bioRxiv. https://doi.org/10.1101/2021.10.04.463034.

## STAR★METHODS

### KEY RESOURCES TABLE

| REAGENT or RESOURCE | SOURCE | IDENTIFIER |
|---|---|---|
| Antibodies | | |
| Anti-ATG8a | Abcam | Cat# ab98830 |
| Anti-NBR1 | Agrisera | Cat# AS14 2805 |
| Anti-GFP | Abcam | Cat# ab290 |
| Anti-mCherry | Abcam | Cat# ab213511 |
| Anti-Actin | Abmart | Cat# M20009H |
| Goat Anti-Rabbit IgG-HRP | Abmart | Cat# M21002L |
| Goat Anti-Mouse IgG-HRP | Abmart | Cat# M21001L |
| Bacterial and virus strains | | |
| *E. coli* DH5α | WEIDI | Cat# DL1001 |
| *Agrobacterium tumefaciens* GV3101 | WEIDI | Cat# AC1001 |
| Y2HGold | Takara | Cat# 630498 |
| Chemicals, peptides, and recombinant proteins | | |
| (N-(3-Triethylammoniumpropyl)-4-(6-(4-(Diethylamino) Phenyl) Hexatrienyl) Pyridinium Dibromide)/FM4-64 | Thermo Fisher | Cat# T13320 |
| LysoTracker™ Deep Red | Thermo Fisher | Cat# L12492 |
| 2′,7′-Bis(2-carboxyethyl)-5(6)-carboxyfluorescein/BCECF | MedChemExpress | Cat# HY-101882 |
| (2′,7′-Bis-(2-Carboxyethyl)-5-(6)-carboxyfluorescein) acetoxymethyl ester/BCECF-AM | Abcam | Cat# ab143463 |
| Propidium iodide/PI | Sigma | Cat# P4170 |
| Dansylcadaverine/MDC | Sigma | Cat# 30432 |
| 3,3′-Diaminobenzidine/DAB | Sigma | Cat# D8001 |
| Nitrotetrazolium Blue chloride/NBT | Sigma | Cat# N6876 |
| 2′,7′-Dichlorodihydrofluorescein diacetate/DCFH-DA | Sigma | Cat# D6883 |
| Concanamycin A/Con A | Sigma | Cat# 27689 |
| TRIzol reagent | Invitrogen | Cat# 15596018 |
| Murashige and Skoog Basal Medium/MS | PhytoTech | Cat# M519 |
| Phenylmethylsulfonyl fluoride/PMSF | American Bioanalytical | Cat# AB01620 |
| Phosophatase Inhibitor Cocktail | Roche | Cat# 4906837001 |
| Dimethyl sulfoxide/DMSO | Sigma | Cat# D8418 |
| 2-[4-(2,4,4-trimethylpentan-2-yl) phenoxy]ethanol/Triton X-100 | Sigma | Cat# T8787 |
| Anti-GFP Magarose Beads | Smart-Lifescience | Cat# SM038100 |
| Critical commercial assays | | |
| PrimeSTAR® GXL DNA Polymerase | Takara | Cat# R050A |
| AxyPrep DNA Gel Extraction Kit | Axygen | Cat# AP-GX-P-250G |
| AxyPrep Plasmid Miniprep Kit | Axygen | Cat# AP-MN-P-250 |
| PrimescriptTM RT Reagent Kit with gDNA Eraser | Takara | Cat# RR037A |
| SYBR Premix Ex Taq qRT-PCR | Takara | Cat# RR420A |
| Hieff Clone® Plus Multi One Step Cloning Kit | Yeasen | Cat# 10911ES20 |
| RIPA lysis buffer | Yeasen | Cat# 20101ES60 |
| NEBuilder® HiFi DNA Assembly | NEB | Cat# E5520S |
| Experimental models: Organisms/strains | | |
| Arabidopsis *pldζ2* | Li et al.[17] | N/A |

(*Continued on next page*)

*Continued*

| REAGENT or RESOURCE | SOURCE | IDENTIFIER |
|---|---|---|
| Arabidopsis *PLDζ2-OE* | Li et al.[17] | N/A |
| Arabidopsis *35S::GFP-ATG8e* | Guan et al.[26] | N/A |
| Arabidopsis *atg7* | Guan et al.[29] | N/A |
| Arabidopsis *35S::PLDζ2-GFP* | This study | N/A |
| Arabidopsis *vatd* | ABRC | SALK_204178C |
| Arabidopsis *vatd/PLDζ2-OE* | This study | N/A |
| Arabidopsis *pldζ2/VATD-OE* | This study | N/A |
| Arabidopsis *pldζ2/GFP-ATG8e* | This study | N/A |
| Arabidopsis *PLDζ2-OE/GFP-ATG8e* | This study | N/A |
| Arabidopsis *VAMP711-GFP* | This study | N/A |
| Arabidopsis *pldζ2/VAMP711-GFP* | This study | N/A |
| Oligonucleotides | | |
| Primers used in this study, see Table S1 | This study | N/A |
| Recombinant DNA | | |
| 35S::PLDζ2-GFP | This study | N/A |
| 35S::HDEL-mCherry | This study | N/A |
| 35S::VATD-mCherry | This study | N/A |
| nYFP-PLDζ2 | This study | N/A |
| VATD-cYFP | This study | N/A |
| PLDζ2-BD | This study | N/A |
| VATD-AD | This study | N/A |
| $VATD^{R46A}$ | This study | N/A |
| $VATD^{K36A}$ | This study | N/A |
| Software and algorithms | | |
| ImageJ | NIH | https://imagej.nih.gov/ij/ |
| GraphPad prism9 | GraphPad | https://www.graphpad.com/features |
| Adobe Illustrator 2021 | Adobe | https://www.adobe.com/products/illustrator/free-trial-download.html |
| AlphaFold v2.2.4 | Evans et al.[52] | https://github.com/deepmind/alphafold |
| PyMol | Schrodinger | https://pymol.org/ |
| Chimera X | RBVI | https://www.cgl.ucsf.edu/chimerax/ |

## EXPERIMENTAL MODEL AND STUDY PARTICIPANT DETAILS

### Plant materials, growth condition, and treatments

All *Arabidopsis* lines used in this study are in Colombia-0 (Col-0) background. The *pldζ2* (Salk_094369) mutant, transgenic plants expressing *35S::GFP-ATG8e* and PLDζ2 (*PLDζ2-OE*) were previously described.[17,26] Mutant *vatd* (SALK_204178C) was obtained from the Arabidopsis Information Resources Center (ABRC) and verified by PCR. The *vatd* and *PLDζ2-OE* were crossed to generate *vatd/PLDζ2-OE*, the *pldζ2* and *VATD-OE* were crossed to generate *pldζ2/VATD-OE*.

Seeds were surface sterilized and vernalized at 4°C in dark for 3 days, then placed on 1/2 Murashige and Skoog (MS) medium and vertically grown at 22°C under 16-h light/8-h dark for 5–7 days with a light intensity of 170 μmol/$m^2$/s using bulbs. After 1 week, the seedlings were transferred to soil for further growth.

For nitrogen and phosphorus starvation, 7-day-old seedlings were transferred to 1/2 MS or nitrogen/phosphorus-deficient MS medium and grown under normal conditions for 5–9 days. For carbon starvation, 7-day-old seedlings were transferred to 1/2 MS or sucrose-deficient MS medium and grown under continuous darkness for 7 days.

## METHOD DETAILS

### Constructs

We utilized the Hieff Clone Plus One Step Cloning Kit (Yeasen) or NEBuilder HiFi DNA Assembly (NEB) to generate constructs according to the manufacturer's instructions. Gene-specific primers, featuring 15-bp extensions that matched the respective vectors,

were listed in Table S1. For plant transformation, full-length cDNA of *PLDζ2* was amplified and subsequently subcloned into pCambia1302 (digested with BglII/SpeI) to generate 35S:PLDζ2-GFP construct. Similarly, full-length cDNA of *VATD* was amplified and subcloned into pCambia1306 (digested with BamHI/EcoRI) to generate 35S:VATD-mCherry construct.

For point mutation, full-length cDNA of *VATD* was amplified and subsequently subcloned into pENTRY (digested with NotI/AscI) to generate pENTRY-VATD construct. Then, site-directed mutagenesis of different sites in VATD was performed using the Q5 Site-Directed Mutagenesis Kit according to the manufacturer's instructions. In yeast two-hybrid (Y2H) assay, cDNAs of *PLDζ2*, *VATD*, $VATD^{K36A}$, and $VATD^{R46A}$ were amplified and subcloned into pGADT7 and pGBKT7 (Clontech), following digestion with EcoRI/BamHI. For Bimolecular Fluorescent Complimentary (BiFC) study, cDNA of *PLDζ2* was amplified and subcloned into pCambia1300S-YN (digested with SmaI/SalI) to generate YN-protein fusion construct; cDNA of *VATD* was amplified and subcloned into pCambia2300S-YC (digested with SmaI/SpeI) to generate protein-YC fusion construct.

### Measurement of chlorophyll contents

Determination of chlorophyll content was performed according to previous description.[28] Arabidopsis leaves were subjected to extraction by immersing in 1 mL of N,N-dimethylformamide for 48 h in darkness at 4°C. The absorbance was recorded at wavelengths of 664 and 647 nm, and the total chlorophyll content was subsequently quantified and adjusted based on the gram fresh weight per sample.

### Detection of autophagy

To investigate the effects of nutrient deficiency, 5-day-old seedlings expressing eGFP-ATG8e grown on 1/2 MS medium were transferred to 1/2 MS medium with or without nutrient supplementation. The primary root cells were examined using a Leica SP8 laser scanning confocal microscope (Germany). For eGFP-ATG8e visualization, the excitation and emission wavelengths were 488 and 507 nm, respectively.

For monodansylcadaverine (MDC) staining, seedlings were subjected to treatment for the specified durations and subsequently immersed in a solution of 0.05 mM MDC (Sigma) in PBS for 10 min, followed by washing three times with PBS at room temperature. The primary root cells were observed using a Leica SP8 laser scanning confocal microscope equipped with a DAPI-specific filter. The excitation and emission wavelengths for MDC were 345 and 455 nm, respectively.

### Transmission electron microscopy (TEM) analysis

The general procedures of preparing conventional samples for transmission electron microscopy (TEM) were according to a previous description with minor modifications.[26] Briefly, leaf sections (~1 $mm^2$) were vacuum-infiltrated and promptly fixed with 2.5% glutaraldehyde in 0.1 M phosphate-buffered saline (PBS) overnight at 4°C. The tissues were washed three times with PBS and post-fixed with 1% OsO4. Samples underwent dehydration in a series of graded ethanol solutions (30%, 50%, 70%, 90%, and 100%). Following dehydration, ethanol was replaced with acetone before embedding the samples in SPI-PON 812 resin. Observation and image capture were carried out using a TEM (Hitachi H-7650 model from Japan, operating at 80 kV).

### Protein extraction and western blotting analysis

Total proteins were extracted from *Arabidopsis* seedlings, *N. benthamiana* leaves, or protoplasts using an ice-cold RIPA lysis buffer containing the following components: 50 mM Tris (pH 7.4), 150 mM NaCl, 1% Triton X-100, 1% sodium deoxycholate, and 0.1% SDS. Additionally, the lysis buffer was supplemented with 1 mM phenylmethanesulfonyl fluoride (PMSF) from Roche. The extraction process involved homogenizing the samples and then placing them on ice for 30 min. Afterward, the homogenates were subjected to centrifugation at 12,000 rpm at 4°C for 15 min. The resulting supernatant was carefully transferred to a new microfuge tube, ready for subsequent electrophoresis. For immunoblotting analysis, total proteins were separated using a 12% SDS-PAGE gel, followed by electroblotting onto a nitrocellulose membrane (Biosharp). The analysis was conducted using antibodies against ATG8a from Abcam and NBR1 from Agersera.

### Yeast two-hybrid (Y2H), Bimolecular Fluorescent Complimentary (BiFC) and subcellular localization analysis

Gal4-based yeast two-hybrid assays were conducted following the manufacturer's instructions (Clontech). Vectors pGADT7 and pGBKT7 were employed to generate the prey and bait constructs, respectively. The constructs were introduced into the yeast strain AH109, which were cultured on synthetic dropout (SD) medium that lacked tryptophan, leucine, and histidine. β-galactosidase (β-gal) liquid assays were performed according to Yeast protocols handbook (Clontech).

For the BiFC (Bimolecular Fluorescent Complimentary) assay, cDNAs of *PLDζ2* and *VATD* were fused either to the N terminus or C terminus of YFP (Yellow Fluorescent Protein). The resultant constructs were transformed into the *A. tumefaciens* strain GV3101 and subsequently infiltrated into the leaves of 5-week-old *N. benthamiana* plants. The infiltrated plants were grown in dark for 48 h, and the fluorescence signals were observed using a Leica SP8 laser scanning confocal microscope (Leica, Germany).

For subcellular localization analysis, cDNAs of *VATD* or *PLDζ2* were fused to mCherry or GFP. The resultant constructs were transformed into the *A. tumefaciens* strain GV3101 and infiltrated into the leaves of either 5-week-old *N. benthamiana* or *Arabidopsis* plants. An ER (Endoplasmic Reticulum) marker, HDEL-mCherry, was transformed to investigate the co-localization of examined proteins.

### Co-immunoprecipitation (Co-IP) analysis

For the process of protein extraction and immunoprecipitation, the following steps were undertaken: 1) Total cell lysate preparation. Cell lysates were prepared in a lysis buffer containing following components: 50 mM Tris-HCl (pH 7.4), 100 mM NaCl, 5 mM EDTA, and 0.5% Triton X-100. To protect the proteins from degradation, a protease inhibitor cocktail from Roche was added to the lysis buffer. 2) Incubation with anti-GFP magnetic microbeads. The cell lysates were incubated with anti-GFP magnetic microbeads overnight at 4°C. This step allowed the selective isolation of proteins bound to GFP-tagged proteins. 3) Washing. After incubation, the samples were washed three times with a buffer composed of 50 mM Tris-HCl (pH 7.4), 100 mM NaCl, and 5 mM EDTA, supplemented with 1× Complete Protease Inhibitor Cocktail. 4) Elution. To release the proteins of interest from the magnetic microbeads, they were eluted by boiling in 2× SDS sample buffer. 5) Separation and analysis. The eluted samples were separated using SDS-PAGE and subsequently analyzed by immunoblotting, employing appropriate antibodies for detection.

### Fluorescence resonance energy transfer with fluorescence lifetime imaging microscopy (FRET-FLIM) assays

The FRET-FLIM experiments were conducted using a Leica STELLARIS laser scanning confocal microscope, which incorporated a white laser and a fluorescence lifetime system. PLDζ2-GFP was used as the donor molecule. The fluorescence lifetime of PLDζ2-GFP alone was measured and served as the negative control. The excitation and emission wavelength were 488 nm or 507 nm, which were chosen to excite and detect the fluorescence emitted by the GFP donor. All measurements were taken from whole-field images containing cells expressing the fluorescent protein at similar expression levels. This uniformity ensured consistency in the experimental conditions.

### Molecular modeling

The structures of the PLDζ2-VATD-VATF complexes were predicted using the AlphaFold server based on AlphaFold 2.3.1 and its multimer prediction model.[52] The predicted structures were visualized using ChimeraX or PyMOL.

## QUANTIFICATION AND STATISTICAL ANALYSIS

To assess the statistical significance of the differences between two groups, a Student's *t*-test was employed. The level of statistical significance is indicated by asterisks (*, $p < 0.05$; **, $p < 0.01$; ***, $p < 0.001$). All detailed statistical details parameters of the experiments can be found in the figure legends. Each experiment was independently repeated for three times, and in each repetition, we analyzed n samples. Statistical analyses were performed using GraphPad Prism.